ROBOTIC HAND POSTURE AND COMPLIANT GRASPING CONTROL USING OPERATIONAL SPACE AND INTEGRAL SLIDING MODE CONTROL

GUIDO HERRMANN[1], JAMALUDIN JALANI[2], MUHAMMAD NASIRUDDIN MAHYUDDIN[3], SAID G KHAN[4] AND CHRIS MELHUISH[5]

ABSTRACT. This paper establishes a novel approach of robotic hand posture and grasping control. For this purpose, the control uses the operational space approach. This permits the consideration of the shape of the object to be grasped. Thus, the control is split into a task control and a particular optimizing posture control. The task controller employs Cylindrical and Spherical coordinate systems due to their simplicity and geometric suitability. This is achieved by using an Integral Sliding Mode Controller (ISMC) as task controller. The ISMC allows us to introduce a model reference approach where a virtual mass-spring damper system can be used to design a compliant trajectory tracking controller. The optimizing posture controller together with the task controller creates a simple approach to obtain pre-grasping/object approach hand postures. The experimental results show that target trajectories can be easily followed by the task control despite the presence of friction and stiction. When the object is grasped, the compliant control will automatically adjust to a specific compliance level due to an augmented compliance parameter adjustment algorithm. Once a specific compliance model has been achieved, the fixed compliance controller can be tested for a specific object grasp scenario. The experimental results prove that the BERUL hand can automatically and successfully attain different compliance levels for a particular object via the ISMC.

[1]G. Herrmann is with the Bristol Robotics Laboratory, Faculty of Engineering, Department of Mechanical Engineering, University of Bristol, BS8 1TR, United Kingdom, mexgh@bris.ac.uk.
[2]J. Jalani is with the Department of Electrical Engineering Technology, Faculty of Engineering Technology, Universiti Tun Hussein Onn Malaysia, 86400, Parit Raja, Batu Pahat, Johor, Malaysia.
[3]M.N.Mahyuddin is with the School of Electrical and Electronics Engineering, Universiti Sains Malaysia, Pulau Pinang, Malaysia.
[4]S. G. Khan is with the Department of Mechanical Engineering, College of Engineering Yanbu, Taibah University, Saudi Arabia.
[5]C. Melhuish is with the Bristol Robotics Laboratory, University of the West of England, Bristol, BS34 8QZ, United Kingdom.

1. INTRODUCTION

Emulating the human hand via a robot hand to perform a grasping task can be challenging[1–4]. Providing sufficient knowledge of the object geometry is an important criterion in order to plan motions and compute successful grasps[5–9]. Interesting results from Akin et al.[6] can assist researchers to plan their grasping technique. These show that over 50% of the required grasps are cylindrical, and it is possible for a three-fingered hand to achieve over 90% of these grasps using a cylindrical design approach for the hand mechanics. Similar results which suggest a cylindrical geometry method can also be found in Geng et al.[7]. This lead Akin et al.[6] to the design of a robotic hand, while Geng et al.[7] derived an approach to transfer human grasping postures to the kinematic positioning of a three fingered hand, using also neural network learning techniques to achieve matching. Thus, for a suitable grasping geometry, a tested cylindrical coordinate system as in Akin et al.[6] and Geng et al.[7] can be very helpful. In contrast, the work in[5,8,9] promotes a spherical reference system for the objects which are to be grasped. Similar to Geng et al.[7] this leads to an analysis of robotic two and three fingered hands for suitable robotic hand postures/positioning, which can be incorporated into robotic hand manipulation processes such as grasping or pinching. The analysis of Gioioso et al.[9] advances over that as it also considers the precise analysis of forces in the human-robot hand mapping strategies. This lead for Gioioso et al.[9] to a detailed simulation analysis of an object model map.

When touching an object, a human hand does not require very high accuracy for the finger positioning and orientation. The grasping task needs to guarantee that the fingers sufficiently surround the object, staying in good contact and creating a suitable ergonomics-inspired posture[10]. As a result of such analysis, the authors of this paper suggested for hand positioning for grasp and for grasping an object-based coordinate system (see early ideas in Jalani, Mahyuddin, Herrmann & Melhuish (2013)[11] and Jalani, Herrmann & Melhuish (2011)[12]); hence, this choice of coordinate system focuses on the object shape. Thus, the control is carried out in relation to the object shape rather than in a global Cartesian coordinate frame. This allows for radial thumb abduction in a pre-grasp positioning exercise of the fingers (all other fingers of our hand follow a cylindrical coordinate system), while finger-object forces are practically controlled using an active compliance control approach, in contrast to a detailed analysis, e.g.[9].

The hand pre-grasping and actual grasping control may be split into a *task* where the finger tips move towards the object, while the fingers overall retain a suitable *posture* to permit good contact in a grasping exercise. A simple way to achieve this desired grasping is by using the operational space approach[13]. The underlying concept of the operational space approach is based on the decomposition of the control signal into *task* and *posture* control. This geometric splitting may have some similarity to the hybrid force/velocity approach in Siciliano et al.[14](pp.396). However, the operational space control approach lends itself to a control approach where a high accuracy finger joint trajectory can be avoided. Exploiting the task controller allows the finger tip to reach a target position of the object through spherical coordinates for the thumb and cylindrical coordinates for the other fingers while the ergonomics-inspired, posture controller keeps a nominal finger posture as much as possible and does not need high accuracy. This allows good enclosure of the object by the controlled fingers. This idea together using in particular an integral sliding mode controller as task compliance controller is elaborated on here in this paper in detail.

Thus, this paper will also provide suggestions to one of the functions required by a robot hand when used in fragile object manipulation or human-robot interaction: the ability to grasp any objects without damage. For this, a compliant control strategy is important to provide such grasping technique[15]. Some effort has been devoted to realize compliant passive grasping[16–19]. Hence, this work was mainly based on passive mechanical compliance which is not easily tunable once practically implemented. In particular for (anthropomorphic) hands and grippers[20,21], the introduction of a mixed compliance system in the joints, actuators and also finger tips can be highly beneficial to the grasping process, but certainly a challenge to manipulation.

Different active compliant control strategies have been proposed by[22–26] . Hybrid force-position control is widely used to handle gripping or grasping of objects[27]; the control approach introduces two states[28,29]. The first state is controlling the positioning error which is also known as controlling an unconstrained mode while the second state is providing force control in a particular direction. Between these two states, there is a transition mode from positioning control to force control. Early controllers resolved this through a switching mode[29] which may be discontinuously achieved. Switching actions may be uncertain and cause instability[30]. More recent solutions have resolved this in a geometric approach,

where the directionality expressed by the kinematics Jacobian defines the directions for position and force control[14,27,30]. Directional force control approaches are ideal in industrial applications[29], but may be generally problematic in scenarios with humanoid robot hands, where the environment is uncertain and multidirectional (although specific exceptions of directional compliance control in robot hands exist[27]).

In contrast, compliance control has been achieved due to the definition of virtual spring-damper systems[23–26,31]. For instance, force/torque sensors have been used to close local force/torque loops to overcome joint flexibilities and uncertainties[23,24,26,32]. These schemes introduce the ability of directly tunable spring-damper interaction via a two loop structure: an internal loop controls a torque tracking structure, while an actively controlled spring-damper system is created in an outer loop. This can be improved by observer-based techniques[33,34] to differentiate external and intrinsic forces and torques (e.g. friction). Nevertheless, accurate model information of the robotic manipulator is required to tune the spring-damper system in the work of[23,24,26,32]. However, a practical robot model is usually not easily identified and uncertain, rendering also the tuned spring-damper system as uncertain. In this respect, a solution to the compliant control problem in grasping has been presented by Zhang et al. (2014)[35] using a combination of an adaptive contact force observer, an environment parameter estimator, an adaptive sliding-mode friction compensator, while Zhang et al.[35] foresee a strong improvement of their results by the future inclusion of an advanced tactile sensor system[36,37]. Considering the comments above, the introduction of robustness to model and environmental uncertainty into compliance control is essential.

In this paper, an integral sliding model control (ISMC) using a model reference idea will be discussed. The reference model will introduce an exact virtual mass-spring-damper system which will determine the compliant control characteristics, i.e. the ISMC approach is not switching between two different states. ISMC (see[38,39] for tracking) is a control approach which can counteract system uncertainties and is particularly useful for mechanical systems with stiction and friction and small negligible flexibilities as the robot hand. For such systems, ISMC is an almost model free control approach, i.e. it permits large system uncertainties and does not require accurate model knowledge as needed for feedback linearization/dynamic inversion schemes; sliding mode control can overcome these

requirements with a high gain control element. Thus, ISMC is robust to model uncertainties and the reference model idea avoids the switching between different states as in hybrid control. Hence, the ISMC controller permits for motion planning and for compliance control due to the inherent model reference characteristics built into ISMC. For compliance, it is desirable that the robot hand is able to adapt to different compliance levels. Humans can effortlessly grasp and manipulate their hand compliance levels for specific objects. This can be realized through the automatic alteration of the reference model in an *initial* tuning process, in particular when a (measured) force signal is exerted on an object.

In contrast to former, seemingly more complex work, this work offers a simplified (power) grasping approach which permits collision-free pre-grasping and grasping with well defined forces using the novel synergetic integration of the following active control techniques:

- Control of a robot hand via the operational space approach using spherical and cylindrical coordinates for pre-grasping positioning and grasping control
- Robust finger (i.e. hand) posture optimization via a robust sliding mode posture controller (recently suggested for a torso robot[40]) which allows for a practical, simple and ergonomically relevant grasping trajectory and which reduces the need for high accuracy.
- Introduction of a novel compliance reference model controller, where the reference model is subject to an external measurement signal and is to be used in the novel context of an Integral Sliding Mode Controller (this avoids scheduling methods, hybrid compliant control approaches and exact robot hand model information).
- Robust compliant control which is non-switching between operating modes, including theoretical guarantees.
- Suggestion of an automatic tuning procedure for the compliance reference model for practical force-object interaction.

Most importantly the results are *practically demonstrated.* Hence, we also extend significantly over our own recent work on compliant grasping (Jalani et al. (2013)[11]; Jalani et al. (2011)[12]), by providing a comprehensive theoretically and practically founded discussion for the complete, combined framework of our robotic hand grasping technique.

2. The Elumotion Hand and its use within a cylindrical and spherical coordinate system

Fig. 1 shows the Bristol Elumotion Robot Hand (BERUL). It is to note that all fingers, i.e. index, middle, ring and small finger consist of three links and three joints except the thumb finger. The thumb has four joints and four links. For the majority of the fingers, these joints are connected through a single, flexible pushrod which is then actuated by a leadscrew mechanism that converts a rotary movement of the electrical motor into a linear movement. Nine servo motors have been attached to various fingers of the BERUL hand. In particular, one motor actuator is used for the small and ring finger and two actuators used for the middle, index and thumb finger. Although the *middle and index fingers* are having two actuators, they follow a planar motion (flexion/extension, see Fig. 1).

In contrast, the thumb end effector motion is more complex due to the two applied actuators and their mechanisms: One actuator is used for the push-rod mechanism (i.e. for palmar abduction), while the other motor introduces rotational motion similar to radial abduction in a human thumb (see Fig. 1).

Since all the fingers are constrained due to the use of the push rod and leadscrew mechanism, the actuation of the first link (proximal phalange) of each finger will create a relational movement of the other links (intermediate and distal phalanges). Measurement of the kinematics of each finger showed that the relationship of the joint movement is sufficiently linear, so that the effect of the push rod constraining the fingers can be modelled similar to a pulley belt system and the discussion can be found in[41] (see Figures 2-3). This allows a reasonably accurate computation of the end positions of each finger tip via forward kinematics in the targeted spherical/cylindrical coordinate system using the motor position, i.e. the first directly actuated joint angle values of each finger, and the linear relationship between each joint angle.

In general, the BERUL hand is able to closely mimic real hand movements and approximate humanlike speeds. For this paper, we focus on the ring, index and thumb finger, as examples of fingers with one and two actuators with planar and non-planar motion.

In order to allow for practical grasping for the BERUL fingers, we exploit the cylindrical and the spherical coordinate system. The cylindrical or the spherical coordinate system can be centered at the object to be grasped (see Figures 2 and 3 for the coordinate

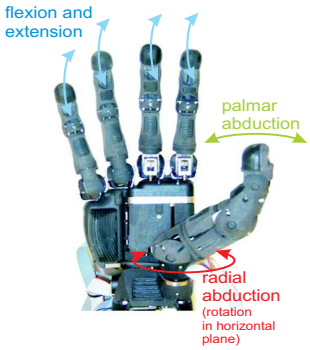

FIGURE 1. An underactuated BERUL hand with available finger motion

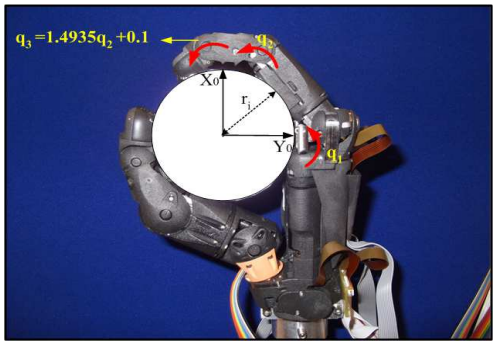

FIGURE 2. Cylindrical coordinate system used for index, middle, ring and small fingers (joint positions in [rad])

system placement). Note that the transformation between joint, Cartesian and Cylindrical/Spherical coordinates follows a standard mathematical calculation. The cylindrical coordinate system is most suited to the index, middle, ring and small fingers, since these fingers often follow a planar movement, even when they are having several actuators. A thumb generally is more versatile in its movements, as it has to move from its initial position around objects (palmar and radial abduction). Thus, spherical coordinates are suited for the thumb. For grasping, it is not necessary to control the joint position of each finger at a high accuracy. Grasping can be easily directed by the radial position r of the finger tip and a preferred posture in case fingers are multi-redundant. Hence, both the cylindrical and spherical coordinates lend themselves to finger control via the radius r.

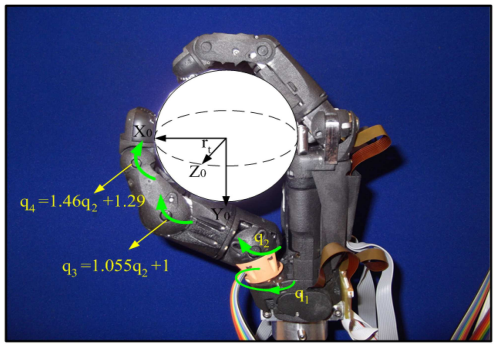

FIGURE 3. Spherical coordinate system used for thumb finger (joint positions in [rad])

3. CONTROLLER STRUCTURE

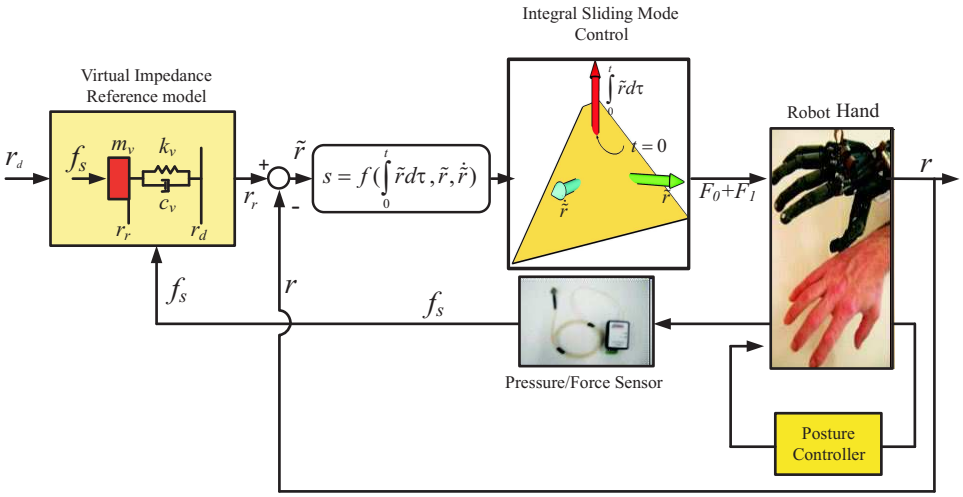

FIGURE 4. Block Diagram of the ISMC to achieve active compliance control for the BERUL fingers

The overall structure for active compliance controller for the BERUL fingers is depicted in Figure 4. We employ the operational space approach, which allows the geometric splitting into task and posture control, creating two parts in the control scheme. The first part is the ISMC based compliance controller for the task, controlling the radial coordinate of each finger in the Cylindrical or spherical coordinate system. The task controller introduces a virtual reference model for compliant (power) grasping in the virtual coordinate r_r, representing a mass spring-damper system considering a virtual mass m_v, spring with coefficient k_v and damping with coefficient c_v subjected to an external force, f_s. This force is sensed through a pressure sensor, creating motion r_r relative to the desired reference

position r_d. Thus, providing a virtual impedance/compliance model for the finger motion under the effect of external forces. The robust integral sliding mode controller enforces that the radial position r of the finger follows r_r at any time (to be explained in Sections 3.1.1 and Section 4). The second part of the controller, the posture controller introduces suitable motion of redundant degrees-of-freedom in particular for the thumb or index finger.

A general model of a robot is

$$M(q)\ddot{q} + V(q,\dot{q})\dot{q} + G(q) + D_f = \tau. \tag{1}$$

where *M*, *V* and *G* provide mass, velocity and gravity terms respectively. The vector D_f represents amplitude limited friction and stiction disturbances and uncertainties; in addition, D_f can also represent forces which result from interaction of the hand with other objects. [i] The torque vector τ represents the external actuating torques affecting each joint. This representation certainly holds for each specific finger for which we develop here the controller, in particular also for the push-rod actuated fingers[39]. It is to point out that in the context of the robot hand, the term $V(q,\dot{q})\dot{q}$ has very little significance. However, the terms $G(q)$ and D_f clearly have significant influence, considering that the practical BERUL hand is to be attached and moved with the robot arm. Moreover, friction and stiction has significant effect due to the pushrod mechanism.

3.1. **Task Control: Model-reference ISMC for compliance and robustness.**

As discussed before, the task coordinate of interest is the radial position r (in the cylindrical/spherical coordinate system), which can be determined by the joint coordinates q. The relevant Jacobian, $J(q)$, of the task coordinate r is defined as

$$J = \frac{\partial r}{\partial q} \tag{2}$$

Considering kinematic redundancy of thumb and ring fingers (i.e. the dimension of the task is strictly less than the dimension of the configuration space), the following pseudo inverse as in[42,43] is used:

$$\bar{J} = M^{-1}J^T(JM^{-1}J^T)^{-1} \tag{3}$$

[i] For control, the forces D_f do not need to be known, as sliding mode control can effectively counteract them. For active compliance, some of these forces will be measurable to be augmented into the compliance control scheme.

Thus, using equation (2) allows us to project joint space dynamics (1) into the task space dynamics of the radius r as follows:

$$\bar{M}(q)\ddot{r} + \bar{V}(q,\dot{q})\dot{r} + \bar{G}(q) + \bar{D}_f = F. \tag{4}$$

where $\bar{M}(q) = (JM^{-1}J^T)^{-1}$, $\bar{V} = \bar{J}^T V - M\dot{J}\dot{q}$, $\bar{G} = \bar{J}^T G$ and $F = \bar{J}^T\tau$. For control, estimates of all system parameters are needed, i.e. $\hat{\bar{M}}$ is the estimate for $\bar{M}$ while $\hat{\bar{V}}$, $\hat{\bar{G}}$ are the two other respective estimates. Friction and other un-modeled forces are $\bar{D}_f = \bar{J}^T D_f$. A typical feedback linearization controller[14] pp.330 with PD controller is:

$$F_0 = \hat{\bar{M}}(q)f^* + \hat{\bar{V}}(q,\dot{q})\dot{r} + \hat{\bar{G}}(q). \tag{5}$$

where $f^* = \ddot{r}_d(t) + K_i r_e + K_s\dot{r}_e$ and r_e is a radial error defined as $r_e(t) = r(t) - r_d(t)$ with $[r_d(t)\ \dot{r}_d(t)\ \ddot{r}_d(t)]$ being the reference trajectory and its time derivatives. Multiplying J in equation (5), the task space control is obtained as follows.

$$\tau_{task} = J^T(F_0 + F_1) \tag{6}$$

where F_1 is to be defined next: Note that the expression (5) contains an estimate of the finger dynamics. These estimates are generically not easily obtained so that the estimation error

$$(\bar{M}\ddot{r}_d + \bar{V}(q,\dot{q})\dot{r} + \bar{G}(q) - \hat{\bar{M}}\ddot{r}_d - \hat{\bar{V}}(q,\dot{q})\dot{r} - \hat{\bar{G}}(q))$$

and also the additional forces $\bar{D}_f$ need to be compensated for by a robust control term. Although these errors can be significant, they are in general amplitude bounded. Thus, the task controller, F_0 (6), is now to be augmented by an integral sliding mode controller, F_1; this will introduce controller robustness and also a reference model behaviour for active compliance control.

3.1.1. *Integral Sliding Mode Controller.* Now, by using the ISMC approach[38], the task control torque is extended by the nonlinear sliding mode term F_1 (6):

$$F_1 = -\Gamma_0\left(\frac{s}{\parallel s \parallel + \delta}\right),\ \delta > 0,\ \Gamma_0 > 0 \tag{7}$$

and

$$s = \dot{r}_e + K_s r_e + K_i\int_0^t r_e d\xi - \int_0^t G_f f_s d\xi - \dot{r}_e(t=0) - K_s r_e(t=0) \tag{8}$$

where $r_e(0)$ and $\dot{r}_e(0)$ are initial conditions. The gain G_f is a positive scalar and f_s is an external force measurement, obtained via specially introduced sensors.[ii] Consider that $\int_0^t(\cdot)d\xi$ are integrals over time with integrant ξ. Moreover, it is easily seen that $s(t=0) = 0$[iii], which is in particular a result of the included initial values $\dot{r}_e(t=0)$ and $r_e(t=0)$. As it will be discussed in greater detail later and as it was indicated in the first paragraph of Section 3, the aim for the controller is to follow a mass-spring damper reference model, which is obtained for $s = 0$.

Following the analysis of[38] , the sliding mode term enforces $s = 0$ for $\delta \to 0+$ and large enough $\Gamma_0 > 0$. The scalar $\delta > 0$ is introduced to avoid any possible chattering in the control action due to the nonlinear sliding mode term. Since $s(t=0) = 0$, it follows for large $\Gamma_0 > 0$ and for $\delta > 0$ that $\|s(t)\|$ is uniformly bounded by a bound proportional to the small value of $\delta > 0$ for all time $t \geq 0$ (see also Appendix for a stability analysis). This in general also reduces high-amplitude control action and chattering[38]. The sliding mode control term F_1 is in particular necessary, when there is model uncertainty (i.e. $\bar{M} \neq \hat{\bar{M}}$, $\bar{V}(q,\dot{q}) \neq \hat{\bar{V}}(q,\dot{q})$, $\bar{G}(q) \neq \hat{\bar{G}}(q)$), unknown uncertainty $\bar{D}_f \neq 0$ and externally sensed forces $f_s \neq 0$. We can expect that any of these terms is bounded so that a practical choice for Γ_0 is possible.

Considering that from $s = 0$ follows $\dot{s} = 0$, sliding motion $s = 0$ implies that the following second order dynamics govern for $s = \dot{s} = 0$ each robot finger:

$$\ddot{r}_e + K_s\dot{r}_e + K_i r_e = G_f f_s, \text{ (if } s = 0) \tag{9}$$

where K_s is a damping coefficient and K_i is a stiffness coefficient of the reference model. Thus, in case sliding motion is satisfied, i.e. $s = 0$, then $\lim_{t\to\infty} r_e(t) = 0$ for a vanishing external force $f_s = 0$ only, following the dynamics of a second order system. For $f_s \neq 0$ and $s = 0$, the external force signal influences the stable second order dynamics, replicating a mass-spring damper system subject to an external force, i.e. in general $r_e \neq 0$; this will be discussed in greater detail in Section 4, using the idea of a virtual model with virtual coordinate r_r. In fact, it is the aim that the radial coordinate follows the virtual model coordinate r_r, i.e. $r = r_r$ for $s = 0$.

[ii] In the case of the BERUL hand, we have used *S*ingle-*P*oint *T*actile *S*ensors (SPTS) which allow for force sensing at the BERUL finger tips; see Section 5 for further detail.

[iii] Note that this is implied from $s(t=0) = \dot{r}_e(t=0) + K_s r_e + K_i \int_0^{t=0} r_e d\xi - \int_0^{t=0} G_f f_s d\xi - \dot{r}_e(t=0) - K_s r_e(t=0) = 0$

It is important to note that in contrast to former work, the introduction of the external signal, f_s, into the reference model (9), in particular also for the operational space control context, creates a novel robust ISMC based compliance control approach.

3.1.2. *Stability and Robustness.* The ISMC has been a well investigated control method due to its robustness[44–46]. Following the definition of s (8), sliding motion (i.e. $s = 0$ is reached) for the ISMC occurs right from the start of the control action, i.e. robustness is guaranteed starting from $t = 0$. Thus, by exploiting this advantage, nonlinear friction and stiction can be eliminated from the BERUL fingers. Moreover, the task motion is unaffected by posture motion. Task motion has priority over posture motion. For this, a rigorous stability analysis for this is carried out in the Appendix using the procedure of[38].

It is important to note, the ISMC can be considered almost a model free design strategy where accurate information of friction/stiction, mass and coriolis forces are not accurately required. Note that this holds as the actuator torques τ (1) directly affects the rigid body dynamics. This is in particular also permissible as sensors and actuators of the BERUL hand are fast and not subjected to any slow dynamics or delays. Moreover, it has been shown that ISMC is superior in the context of trajectory following for the BERUL hand subjected to friction, in comparison to many other control methods[39,41].

3.2. **Posture Control For Grasping .**

The posture controllers are meant to regulate the remaining degrees of freedom, which are not controlled by the task controller. The index and the thumb fingers have both two actuators to control their finger tip position in terms of radial position and posture. The idea for the posture is to minimize a cost function, $U(q)$, which guarantees a certain 'optimal' (nominal) positioning of the redundant degrees of freedom. In case of[13] and[40] , this was an effort minimizing cost function based on the effects of gravity. This has induced human like motion for a robot torso and arm control. In our case, the effects of gravity are too strongly varying with the hand movement so that a more specific hand posture cost independent of gravity is needed here.

We consider the thumb and the index finger which have two actuated degrees of freedom, q_1 and q_2. The geometric projection matrix

$$N^T = (I - J^T \bar{J}^T) = (I - J^T (JM^{-1}J^T)^{-1} JM^{-1}) \tag{10}$$

is important for the posture task, as it defines the null space of the task controller (Note that the ring finger discussed here in this paper has only one actuator where all joints are connected through a push rod. For this finger $N = 0$.). It is easily seen that $\bar{J}^T N^T = 0$ and $N^T N^T = N^T$.

The overall control signal for a BERUL finger can be written as:

$$\tau = J^T(F_0 + F_1) + \hat{N}^T(-K_{dp}\dot{q} - K_{SL}\frac{\hat{M}\hat{s}}{\parallel \hat{s} \parallel + \delta_{SL}}) \tag{11}$$

where $K_{dp} > 0$, $K_{SL} > 0$, $\delta > 0$ and $\hat{N}$ is computed from (10) using the mass estimate $\hat{M}$ instead of the exact value M. The variable $\hat{s}$

$$\hat{s} = B(\dot{q} + K_v(\frac{\partial U}{\partial q})^T) \tag{12}$$

introduces a sliding mode variable for the posture control where

$$B = (I - J^T(JJ^T)^{-1}J). \tag{13}$$

The matrix B is a projection matrix similar to N^T, which is complemented by

$$\hat{B} = J^T(JJ^T)^{-1}J. \tag{14}$$

Hence, for instance, it is easily verified that $JB = 0$ and $B + \hat{B} = I$, which subsequently also implies $\tilde{B}B = 0$, $B\tilde{B} = 0$, $BB = B$ and $\hat{B}\hat{B} = \hat{B}$. In the ideal case, the nonlinear sliding mode term enforces $\hat{s} = 0$ for $\delta_{SL} \to 0+$. This is achieved irrespective model uncertainties and un-modelled forces (e.g. gravity, friction and stiction), which makes the posture control robust to system uncertainty[40] in contrast to[13] (see also a robustness analysis of the controller in the Appendix using[40]). Thus, this robust gradient descent approach minimizing $U(q)$ is preferred for our hand control case.

3.3. **Posture control with enforced gradient descent $\hat{s} = 0$.**

It was mentioned before that the task control has priority over the posture, i.e. the task control is not influenced by the posture control. In contrast, the posture control is influenced by task motion. Thus, although $\hat{s} = 0$ can be achieved within finite time (see Appendix for analysis), the minimizing effect of the posture controller is best seen for the case $B = I$ (see also[40]). This is only possible if all degrees of freedom q_1 and q_2 are part of the posture control scheme (which is in general not the case).

The general case, implies from $\hat{s} = 0$:

$$B\dot{q} = -K_v B \left[\frac{\partial U}{\partial q}\right]^T. \tag{15}$$

Thus, considering that

$$\dot{U}(q) = \left[\frac{\partial U}{\partial q}\right] \dot{q} = \left[\frac{\partial U}{\partial q}\right] (B + \hat{B})\dot{q} \tag{16}$$

we obtain

$$\dot{U}(q) = -K_v \left|\left|\frac{\partial U}{\partial q} B\right|\right|^2 + \left[\frac{\partial U}{\partial q}\right] \hat{B}\dot{q}. \tag{17}$$

This shows that the sliding mode element in the posture controller introduces gradient descent via $-K_v \left|\left|\frac{\partial U}{\partial q} B\right|\right|^2$ to minimize $U(q)$. In particular, for $B = I$, $\dot{U}(q) = -K_v \left|\left|\frac{\partial U}{\partial q}\right|\right|^2$. In general, $B \neq I$ and $\hat{B} \neq 0$ which implies that the cost function is still decreasing but a trade off has to be made due to the task control, which has priority over the posture controller. This is observed in (17), where the last term is generally non-zero for $\hat{B} \neq 0$. Hence, a cost optimization of U is limited/influenced by the task of the finger end position.

To note again, the control (11) shows for a generic manipulator problem that $\hat{s} = 0$ is achieved for large enough gain $K_{SL} > 0$ (see Appendix and the work[40]), in particular when the robot manipulator is affected by friction and the controller lacks model knowledge. Thus, a robust posture control (11) is defined.

4. Compliance Control And Model Reference Behavior

4.1. **Compliance.**

For compliance, we reconsider the sliding variable s (8) and its derivative:

$$\dot{s} = \ddot{r}_e + K_s \dot{r}_e + K_i r_e - G_f f_s \tag{18}$$

When sliding motion is achieved, then $s = 0$ and in particular $\dot{s} = 0$. For $\dot{s} = 0$, the error dynamics are defined by the (damping) constant K_s, the (spring) constant K_i and the external force measurement signal f_s introduced via the input distribution gain G_f, i.e. (9). This defines a reference model (9) allowing for active compliance control via the external force signal f_s.

This contrasts to the recent use of ISMC, e.g.[38,39], where the sliding mode dynamics generally define a nominal closed loop behavior without external signals. This is an important tool as the controller guarantees a well defined level of compliance despite the high degree of uncertainty and friction in the robot hands.

In practice, it is not always possible to obtain $s = 0$ (8) at all times. Thus, it is sensible to introduce a virtual model similar to (9), as (9) only holds for $s = 0$. A virtual demand model with the coordinate r_r for this is

$$\ddot{r}_r = -K_s\dot{r}_r - K_i r_r + G_f f_s + K_s\dot{r}_d + K_i r_d + \ddot{r}_d. \tag{19}$$

using the initial conditions $r_r(t=0) = r(t=0)$ and $\dot{r}_r(t=0) = \dot{r}(t=0)$. This implies for $R_e = r_r - r_d$ that

$$\ddot{R}_e + K_s\dot{R}_e + K_i R_e = G_f f_s,$$

which is identical to the reference model of (9) (note again that (9) is only valid once $s = 0$).

Thus, this implies from (8) and after subtraction of the integrated equation of (19) the following

$$\begin{aligned} s(t) &= (\dot{r}(t) - \dot{r}_r(t)) + K_s(r(t) - r_r(t)) + K_i \int_0^t (r(\xi) - r_r(\xi))d\xi \\ &\quad -(\dot{r}(0) - \dot{r}_r(0)) - K_s(r(0) - r_r(0)), \\ &= (\dot{r}(t) - \dot{r}_r(t)) + K_s(r(t) - r_r(t)) + K_i \int_0^t (r(\xi) - r_r(\xi))d\xi \end{aligned} \tag{20}$$

Hence, for $s = 0$, $\tilde{r} = r_r - r = 0$ and in particular $\tilde{r}(t) = 0$ for all $t > 0$ when $r_r(t=0) = r(t=0)$, $\dot{r}_r(t=0) = \dot{r}(t=0)$. Thus, the joint coordinates r have to follow the virtual demand r_r in the ideal case of $s = 0$, given an original demand r_d. Hence, the relationship of (20) is an important alternative expression for s (8) focussing on the reference model of (19) which is equivalent to (9) for $s = 0$. Thus, it is used here only for analysis, while the expression (8) is to be used in the implementation.

4.2. **A Virtual Mass-Spring Damper Reference and Computation of Compliance Level for an Object.**

It is noted that for $s = 0$ follows from (9) that $r_r = r$ and

$$\frac{r_e(s)}{f_s(s)} = \frac{G_f}{s^2 + K_s s + K_i} \tag{21}$$

where $K_s = 2\zeta\omega_n$ and $K_i = {\omega_n}^2$. The scalars ζ and ω_n are damping ratio and natural frequency respectively. Thus, different K_s, K_i and G_f to be used in order to obtain compliance levels.

The reference model cannot be arbitrarily determined and it needs to be bespoke, suitably adjusted to the context of the object handled by the robot fingers, in particular when considering the steady state force equilibrium. For this, let us consider the following mass-spring damper system:

$$\ddot{r}_e + \frac{c_v}{m_v}\dot{r}_e + \frac{k_v}{m_v} r_e = \frac{1}{m_v} f_s \tag{22}$$

where m_v is a virtual mass of the spring, c_v is a virtual damping constant and k_v is a virtual spring constant. By equating equation (22) with equation (9) the following relations are obtained.

$$\frac{c_v}{m_v} = 2\zeta\omega_n = K_s;\ \frac{k_v}{m_v} = {\omega_n}^2 = K_i;\ G_f f_s = \frac{1}{m_v} f_s \tag{23}$$

where $G_f = \frac{1}{m_v}$. The target is now to determine c_v, k_v and m_v via suitable practical tests and design requirements for compliance and transient behavior. We may assume that ζ and ω_n are given to establish a suitable transient behavior, which fixes $\frac{c_v}{m_v}$ and $\frac{k_v}{m_v}$. The sensitivity to the measured force is adjusted through the input gain $G_f = \frac{1}{m_v}$.

It is now the aim to find G_f in a semi-automated process. This is to be carried out once, before any new compliant interaction task, which is to ensure safe interaction after this initial tuning process. The software-implemented process is given as follows (See also Figure 5).

(1) G_f is set to a significantly large initial value which will make the reference model highly sensitive to any external signal f_s. A task controller is initiated for a constant demand r_d. For the finger to reach r_d, it would have to penetrate the touched object, which is assumed to be stationary.

(2) The finger is controlled via r_d so that it touches the object, as the demanded radius r_d is set smaller than the actual radius of the object. Any significant high pressure during the touching process is to be avoided by the compliance controller and an adjusted value r_r (19). The initial large $G_f > 0$ makes the reference model highly sensitive to a touching interaction of the object with the finger. Once the finger has

contacted the object, a sensor signal f_s is measured. Since a constant target value for r_d is set, the sensor signal f_s is steadily increasing.

(3) A level F_{L1} is used to *initiate the tuning process* for G_f. Hence, once the sensor signal f_s is larger than F_{L1} for a well-defined period of time (4-5 sampling instances), the value of G_f is very slowly decreased in an automated fashion. This will make the reference model less sensitive to f_s, increase the magnitude of f_s and force r_r to be closer to r_d (19).

(4) Once the force sensor signal, f_s, has surpassed a level F_{L2}, ($F_{L2} \geq F_{L1}$) the decreasing value of G_f is kept fixed. Hence, the choice F_{L2} *defines the maximum force applied to the object and therefore determines the compliance level of the reference model* via the fixed parameters K_s, K_i and G_f. These values are now available for further use.

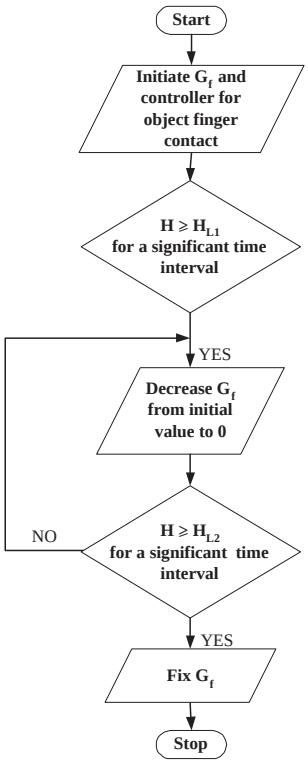

FIGURE 5. Automated input distributed gain (G_f) (see itemized explanation)

In summary, the process above allows to introduce a compliance reference model for a specific object-finger force interaction force level F_{L2} in a semi-automated manner. This

is to be carried out once for the reference model to be used later for the specific class of object in robot-object interaction.

5. Experimental Setup and Results

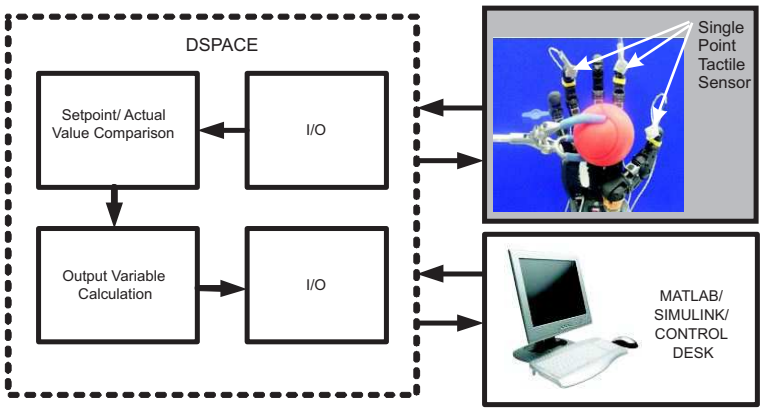

FIGURE 6. Experimental setup for BERUL finger

The experimental setup for the BERUL fingers is shown in Fig. 6. As a real-time interface, the dSPACE DS1006 Controller Board is used to interact with the BERUL fingers for rapid prototyping of control algorithms. Hence, the motors actuating the pushrod are driven by an EPOS brushless DC motor driver unit and the angular position of the motor is read by means of an incremental encoder. The EPOS motor drivers at each joint are in fact connected to the dSPACE system by a CAN communication bus. The control signals sent via this CAN bus, are managed by a CANopen communication protocol using a periodic synchronisation signal. This allows a deterministic communication to be established in the CAN network without polling. The control loops are running at a sampling frequency of 1 kHz. Note that any computational effort needed for the nonlinear controller is negligible at this sampling frequency.

The results are divided into five different cases. Case 1 looks at the compliant behaviour of the task controller determined by a fixed reference model. Case 2 investigates the effectiveness of the posture controller, which is important for pre-grasping/object-approach hand posture and positioning. Case 3 is looking at task tracking performance of all the fingers, while posture control ensures correct finger positioning for pre-grasping and grasping. Case 4 shows the performance for different compliance levels in the task controller for a specific object. A $hard$ rubber ball (Figure 7(a)) is used to show the results for Case 4.

Case 5 demonstrates the effectiveness of the ISMC compliance controller for different objects. A $hard$ spongy ball (Figure 7(b)) and a $soft$ balloon (Figure 7(c)) are used to show the results for Case 5.

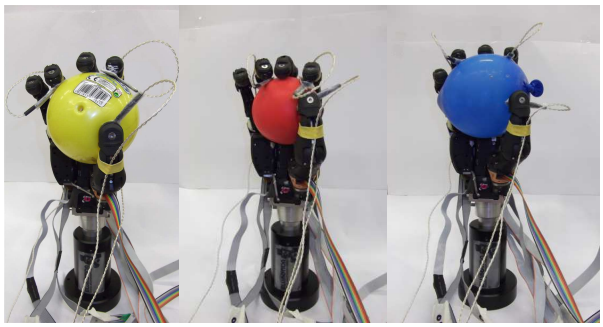

(a) Rubber Ball (b) Spongy Ball (c) Balloon

FIGURE 7. Tested objects for practical compliance

The ConTacts C500 *S*ingle-*P*oint *T*actile *S*ensors from PressureProfile Inc.[47] (see Figure 6) are mounted on the fingers in particular for the thumb, the index and the ring fingers; they are used to grasp various objects. Thus, only 3 fingers have been tested namely ring, index and thumb finger for practicality and also due to availability of three SPTSs only (It is not unusual to use three finger hands for practical grasping[6]). The SPTS has a diameter of 1 cm and it has a pressure output voltage relationship which can be approximated to about 1379 Pa = 2 psi per 1 V. Considering the area of the sensor this relates to 4.33 N per 1 V across the pad of the SPTS. The SPTS uses capacitive-based conformable pressure sensors to accurately and reliably quantify applied forces. The analog voltage outputs are fed back into the controller for force measurement to be used for f_s (8).

5.1. **Compliance/Impedance for different stiffness and damping - Case 1.**

The analysis of different compliance characteristics for the ring finger are discussed in this section. It is noted that from (23) follows $K_s = 2\zeta\omega_n$ and $K_i = \omega_n^2$. Thus, different K_s and K_i are selected in order to observe compliance levels, while $G_f = 2.28$ remains fixed.

The compliance model reference behavior is experimentally tested by exerting a calibrated force of the same amplitude to be sensed by the ISMC algorithm as shown in Fig. 8(a), Fig. 8(c) and Fig. 8(e). This is easily achieved by capping the externally sensed short

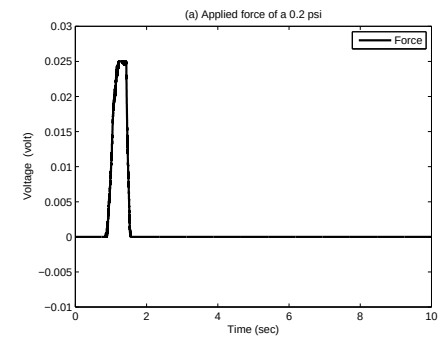

(a) Pressure sensor

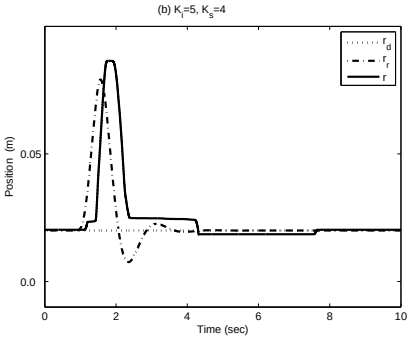

(b) Position r, r_r and r_d for $K_i = 5$, $K_s = 4$ and $G_f = 2.28, \omega = 2.23, \zeta = 0.894$

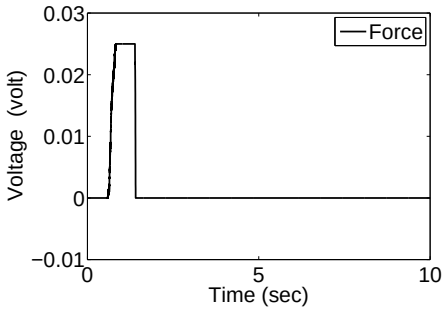

(c) Pressure sensor

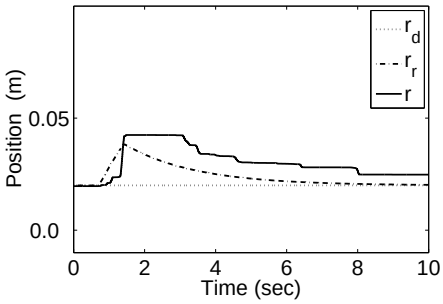

(d) Position r, r_r and r_d for $K_i = 5$, $K_s = 25$ and $G_f = 2.28, \omega = 2.23, \zeta = 5.59$

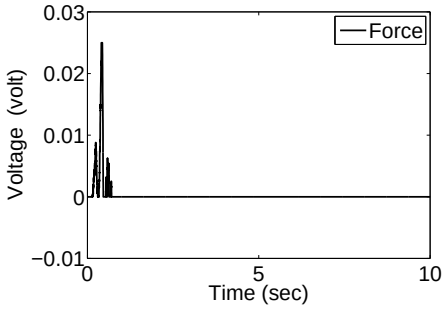

(e) Pressure sensor

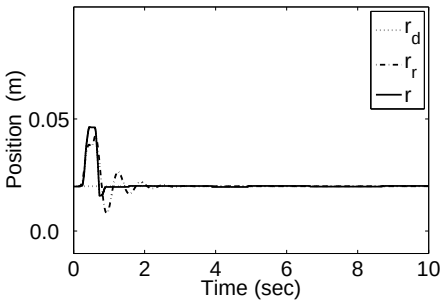

(f) Position r, r_r and r_d for $K_i = 25$, $K_s = 4$ and $G_f = 2.28, \omega = 5, \zeta = 0.4$

FIGURE 8. Compliance/Impedance performance for thumb and applied pressure amplitude of 0.2 psi

burst force to the amplitude of 0.025 V (=0.108N). For this, the actual demand r_d is kept constant. In Fig. 8(b), Fig. 8(d) and Fig. 8(f), compliance control results are provided, r_d is the original demand, r_r is the demand calculated from the virtual reference model (19) for the actual radial position r is for the thumb finger. Thus, we use a spherical coordinate

system in the case of the thumb as this will ultimately work for radial thumb abduction (in contrast to ring and index finger using cylindrical coordinates). The results clearly show that our design for a reference model is effective in creating active compliance. This can be seen in Fig. 8(d) where by increasing K_s (i.e. increasing the damping coefficient to $\zeta = 5.59$) the compliance controller becomes sluggish. On the other hand by increasing K_i (i.e. increasing the spring coefficient), the compliance becomes more stiff and fast, as seen in Fig. 8(f).

5.2. **Posture Controller Parameters and Results - Case 2.**

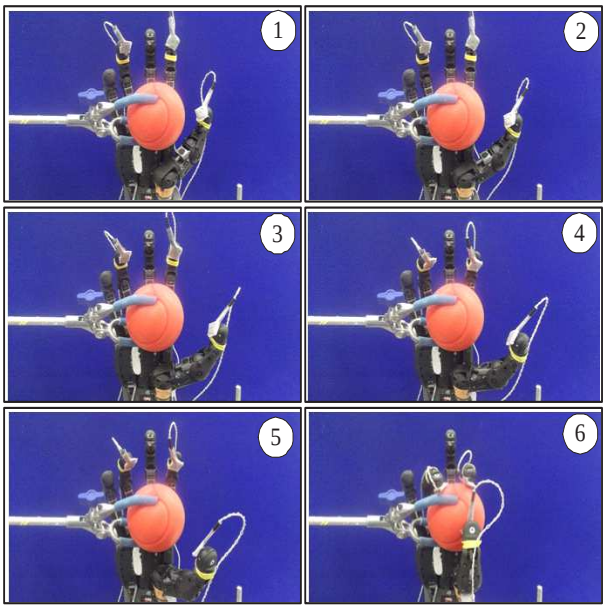

FIGURE 9. Approach and grasp scenario; cylindrical coordinate space for index and ring fingers; spherical coordinate space for thumb finger (pre-grasping in subfigure 1-5; grasping in subfigure 6)

For the experimental case 2, the robot hand is kept in upward position, while a tube holder is used to hold a ball with a diameter of about 6 cm slightly to the left of the centre point of the spherical coordinate system used for the thumb (see Figure 9, subfigure 1). The gains used for the posture controller in particular for the index finger are $K_{dp} = 2$, $K_{SL} = 16$, $K_v = 4$, $w_1 = 3$ and $w_2 = 3$. The nominal joint positions ϕ_1 and ϕ_2 are chosen as $\phi_1 = 0.45\,rad$ and $\phi_2 = 1.5\,rad$. This in fact defines a finger in a slightly bent, almost-open hand position. Thus, once the task controller is enabled (task control has

priority over posture), the nominal "almost-open" finger posture (following ergonomics studies in [10]) will guarantee that the finger encloses the object; this is visible in the motion capture of Figure 9, subfigures 2-5. (Note that the ring finger does not require any posture control.) On the other hand, the gains for the thumb finger are $K_{dp} = 2$, $K_{SL} = 160$, $K_v = 4$, $w_1 = 2$ and $w_2 = 2$. The nominal positions of the thumb are $\phi_1 = -2.5\ rad$ and $\phi_2 = 1.5\ rad$. They enforce for the thumb finger to move from an initial (open hand) position (see Figure 9, subfigures 1-5) to a position where the thumb is in front of the object (Figure 9, subfigure 6). This permits, for instance, correct positioning of the thumb before grasping, to assure a safe enclosure of an object to be grasped. Hence, although the task controller has priority to achieve the correct *radial finger tip position*, the posture controller guarantees that the redundant degrees of freedom of the hand permit practical, ergonomics-based grasping positions [10], which is not achievable via task control only.

5.3. **Tracking Results - Case 3.**

In this case, the task controller is assessed without considering any hand-object interaction to allow accurate task control tracking assessment. Thus, the hand is again kept upright, while no object is brought into the vicinity of the hand. This will imply $f_s = 0$ and $r_r = r_d$ in this case. Considering the results from Case 2, the reference model parameters (9) have been chosen as follows: $K_s = 8$ and $K_i = 18$ which implies $\omega_n = 4$ and $\zeta = 0.9$. Hence, the choice of $\omega_n = 4$ and $\zeta = 0.9$ will guarantee an approximate settling time of 1 second for a slightly underdamped reference model. The results show that, while maintaining a desired posture motion (e.g. Figure 9), the tracking of r can be achieved (see Figure 10). Moreover, the results also show that the fingers satisfactorily follow a desired trajectory (i.e. r follows r_d) during the hand opening and the hand closing period. More specifically, the task controller performance is very good despite the posture controller forces the index finger to retain an "open" finger position as much as possible. This is clearly a result of the operational space approach, i.e. the prioritization of the task controller over the posture control.

5.4. **Compliance level results for an object - Case 4.**

The automated compliance level search procedure of Section 4.2 is investigated for grasping of a $hard$ rubber ball with a diameter of about 8 cm (see Figure 7(a)). The ball

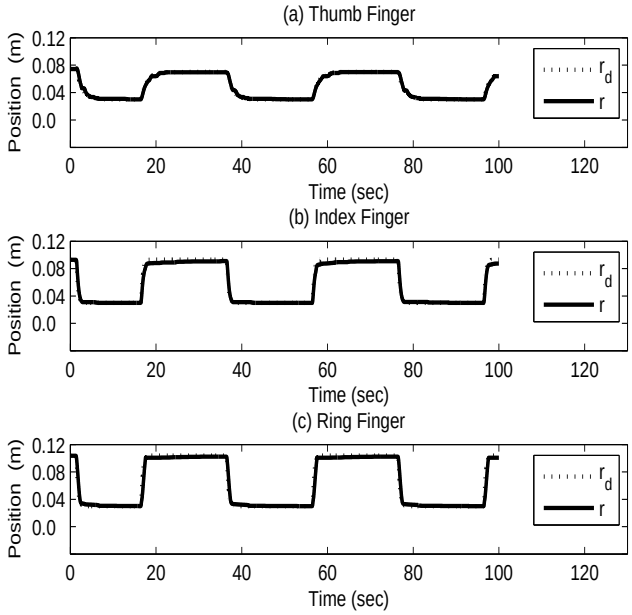

FIGURE 10. a) r_d-tracking for thumb finger in Spherical coordinates, (b)and(c) r_d-tracking for index and ring fingers in cylindrical coordinates

is first lightly held by the tube holder, slightly left of the spherical coordinate centre, while the tube holder is then carefully removed to test the grasping process (see Figure 9 versus Figure 5). We have investigated two different options for the permissible contact forces F_{L2}. The level $F_{L2} = 0.01\ V(0.0433\ N)$ and later $F_{L2} = 0.04\ V(0.1733\ N)$. These force levels are chosen to enable object grasping without damaging the object (and also the robot hand). The lower force $F_{L2} = 0.01\ V(0.0433\ N)$ permits a very light grasp, just avoiding object slippage.

The results reveal that a suitable reference model for both F_{L2} can be satisfactorily achieved for both levels as shown in Figure 11 and Figure 12 within the first 10 seconds. It shows that different levels of compliance are feasible for the same object. Moreover, the suggested technique to capture an appropriate G_f is reliable since it can be repeated.

Moreover, in Figure 11 and Figure 12, the compliance control action for fixed $G_f = const.$, $G_f > 0$, is assessed. This can be seen after a period of 60 seconds. Note that during the period from 40 seconds to 60 seconds the fingers are open (i.e. not grasping).

It is also visible, in particular for the ring finger (Figures 11 and 12) that the pressures exerted on the object must be higher for $F_{L2} = 0.04\ V(0.1733\ N)$ in contrast to $F_{L2} =$

$0.01V(0.0433\ N)$ since r_d and r_r are slightly closer together. Generally, the gain G_f is larger for $F_{L2} = 0.01\ V(0.0433\ N)$ in relation to $F_{L2} = 0.04\ V(0.1733\ N)$ (see Tables I and II). Note the rather nonlinear relationship between F_{L2} and G_f for the two options. The decrease of G_f from $F_{L2} = 0.01\ V(0.0433\ N)$ to $F_{L2} = 0.04\ V(0.1733\ N)$ appears to be small, but is was found to be a repeatable result. The small difference in G_f for $F_{L2} = 0.04V(0.1733\ N)$ and $F_{L2} = 0.01V(0.0433\ N)$ may be explained by the material properties of the touched object.

TABLE I. Desired Force for level 0.0433 N (0.01V)- hard rubber ball

$Finger$	G_f	F_{L2} (V)
Thumb	9.519	0.01
Index	9.959	0.01
Ring	9.993	0.01

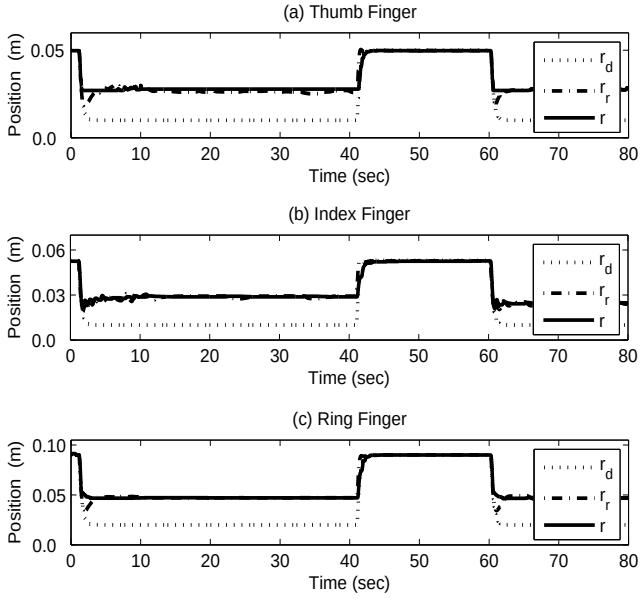

FIGURE 11. Compliance performance for level 0.0433 N (0.01V)

5.5. **Compliance level results for different objects - Case 5.**

The automated compliance level search procedure of Section 4.2 is again used to find the compliance model investigated for a $hard$ spongy ball (diameter $\sim$ 6 cm) and a $soft$

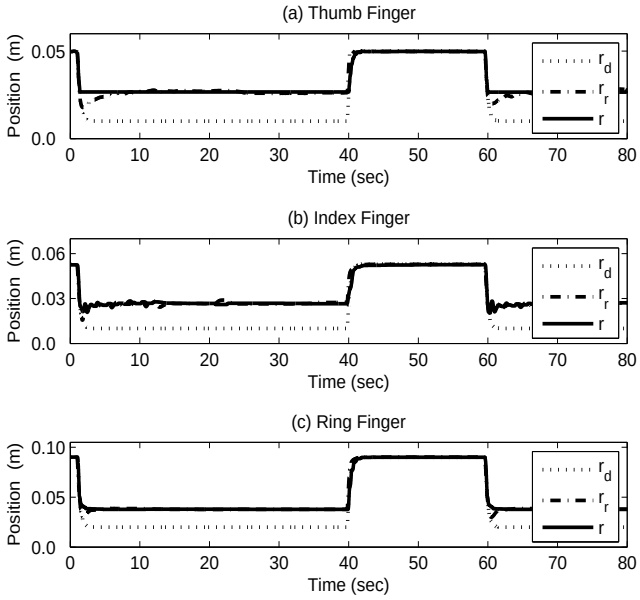

FIGURE 12. Compliance performance for level 0.1733 N (0.04V)

TABLE II. Desired Force for level 0.1733N (0.04V) - hard rubber ball

$Finger$	G_f	F_{L2} (V)
Thumb	8.349	0.04
Index	9.851	0.04
Ring	9.118	0.04

balloon (diameter $\sim$ 7 cm). The results show that the automatic adjustment approach is feasible to classify compliance models for a $hard$ spongy ball as shown in Table III in contrast to a $soft$ balloon as shown in Table IV. The experimental process is identical to Case 4, i.e. the tube holder is used to position the touched object, while it is later removed to test if the object is securely grasped.

We have chosen $F_{L2} = 0.02V$, a force level which enables grasping of both objects. Quite clearly, a soft balloon requires a smaller G_f for the reference model, as it is easier compressed. Hence, the fixed force level of $F_{L2} = 0.02V$ (see Table III and IV) implies a smaller G_f, i.e. a 'stiffer' reference model.

TABLE III. Desired Force for level 0.0866 N (0.02V) - hard spongy ball

$Finger$	G_f	F_{L2} (V)
Thumb	9.810	0.02
Index	9.969	0.02
Ring	9.998	0.02

TABLE IV. Desired Force for level 0.0866 N (0.02V) - soft balloon

$Finger$	G_f	F_{L2} (V)
Thumb	9.689	0.02
Index	9.866	0.02
Ring	9.401	0.02

5.6. **Discussion.**

It is important to note that the results of this paper provide a robust, applicable approach which allows practical (power) grasping and well-measured, object-specific robust compliance. This is enabled by a synergy of techniques: operational space approach, robust integral sliding mode control (ISMC) in task motion for introduction of compliant control reference models and optimal posture motion to guarantee posture. As posture motion is secondary to task motion, any possible issues concerning work space are resolved indirectly: the posture control will attempt to optimize the desirable, ergonomically justified cost, while adhering to any limitations given by the hand kinematics. At the same time, compliant grasping is achieved by the ISMC-based active compliant control. The compliant controller is following a well defined reference model, while it is fully independent from significant model parameter uncertainty of the BERUL robot hand. This for instance contrasts the work of of Gioioso et al.[9], where forces are dependent on finger and object coordinate and motion relative to each other, resulting from a detailed theoretical analysis.

6. CONCLUSIONS

In this paper, we propose a novel approach for active compliance control via Integral Sliding Mode Control (ISMC). The ISMC allows us to introduce a model reference approach where a virtual mass-spring-damper system can be used to design a compliant control. The finger motion is controlled by a posture controller and a task controller as parts of an operational space controller. Both controllers use sliding mode methods to ensure robustness. Results show that the task controller can achieve indeed good tracking

performance despite high levels of stiction and friction. The idea of using cylindrical and spherical coordinates and the posture controller of the index and thumb finger guarantees that both fingers move around the touched object without collision. This will allow for approach for (power) grasping and practical (power) grasping via the chosen geometry.

The tactile pressure sensors are mounted on the BERUL fingers to permit only a desired force level to affect any object. The effectiveness of the compliant control when grasping similar object has been successfully demonstrated at different desired force levels via an automated tuning procedure. The method is also suitable for achieving compliance levels for different objects. The automated tuning process has shown that reference models for particular force levels and different objects can be easily achieved. It shows that higher desired forces require a 'stiffer' reference model. For a given constant interaction force, soft objects imply also a 'stiffer' reference model as these objects are easily compressed.

ACKNOWLEDGMENT

This project received partially funds from CHRIS (Cooperative Human Robot Interaction Systems, 2008-2012) project of the European Commission's Seventh Framework Programme (FP7). This research was also partially funded by the Malaysian Government.

APPENDIX A. STABILITY ANALYSIS

The appendix summarizes in a brief manner a stability argument for the control scheme, considering ideas of[38] and[40].

A.1. **Task Motion.**

Fact 1. The task motion is not influenced by the posture controller if the mass estimate $\hat{M} = M$ is correct. ∘

This is known from operational space control[13,42,43].

Proof: This fact is easily obtained from the following line of argumentation:
The combined controller of task and posture controller is given by (11), while the task motion trajectory r is described by the dynamics of (4). Note that the dynamics of (4) are the result of a nonlinear transformation. In particular, the virtual input force/torque F is

defined by $F = \bar{J}^T \tau$, where $\bar{J}$ is defined in (3). Note that $\bar{J}^T N^T = 0$. Moreover, $\hat{N} = N$ for $\hat{M} = M$. Thus, using the definition $F = \bar{J}^T \tau$, it follows from equation (11)

$$
\begin{aligned}
(24) \qquad F &= \bar{J}^T \tau \\
&= \bar{J}^T \left(J^T (F_0 + F_1) + N^T (-K_{dp} \dot{q} - K_{SL} \frac{\hat{\bar{M}} \hat{s}}{\parallel \hat{s} \parallel + \delta_{SL}}) \right) \\
&= F_0 + F_1
\end{aligned}
$$

■

Thus, task motion is not influenced by the posture controller. The next step is to show robust stability of the task control, in particular that the sliding mode variable s (8) remains 0 for $\delta = 0$:

Lemma 1. *Provided that Γ_0 is large enough, the sliding mode variable s remains within a small compact set containing the origin 0. For $\delta = 0$, s remains 0 at all times.* •

The proof of this Lemma is based on ideas of[38]:

Proof: At first, consider the sliding variable s (8) and its derivative $\dot{s}$:

$$
(25) \qquad \dot{s} = \ddot{r}_e + K_s \dot{r}_e + K_i r_e - G_f f_s,
$$

The control law $F = F_0 + F_1 + \bar{J}^T (\hat{N} - N)^T (-K_{dp} \dot{q} - K_{SL} \frac{\hat{\bar{M}} \hat{s}}{\parallel \hat{s} \parallel + \delta_{SL}})$ from (5) and (7) implies for the task control dynamics of (4)

$$
\begin{aligned}
\bar{M} \ddot{r}_e + \bar{M} K_s \dot{r}_e + \bar{M} K_i r_e - \bar{M} G_f f_s \quad = \quad & (\hat{\bar{M}} - \bar{M}) f^* + (\hat{\bar{V}}(q, \dot{q}) \dot{r} - \bar{V}(q, \dot{q}) \dot{r}) \\
& + (\hat{\bar{G}}(q) - \bar{G}(q)) - \bar{D}_f - \bar{M} G_f f_s \\
& + \bar{J}^T (\hat{N} - N)^T (-K_{dp} \dot{q} - K_{SL} \frac{\hat{\bar{M}} \hat{s}}{\parallel \hat{s} \parallel + \delta_{SL}}) \\
& - \Gamma_0 (\frac{s}{\parallel s \parallel + \delta}),
\end{aligned}
$$

or equivalently

$$
\begin{aligned}
\bar{M} \dot{s} \quad = \quad & (\hat{\bar{M}} - \bar{M}) f^* + (\hat{\bar{V}}(q, \dot{q}) \dot{r} - \bar{V}(q, \dot{q}) \dot{r}) \\
& + (\hat{\bar{G}}(q) - \bar{G}(q)) - \bar{D}_f - \bar{M} G_f f_s \\
& + \bar{J}^T (\hat{N} - N)^T (-K_{dp} \dot{q} - K_{SL} \frac{\hat{\bar{M}} \hat{s}}{\parallel \hat{s} \parallel + \delta_{SL}}) - \Gamma_0 (\frac{s}{\parallel s \parallel + \delta}),
\end{aligned}
$$

Consider the following function $V_s = \frac{1}{2}s^T s$. Computing the temporal derivative, it follows:

$$\begin{aligned}
\dot{V}_s &= s^T \dot{s} \\
&= s^T \bar{M}^{-1} \left((\hat{\bar{M}} - \bar{M}) f^* + (\hat{\bar{V}}(q,\dot{q})\dot{r} - \bar{V}(q,\dot{q})\dot{r}) \right) \\
&\quad + s^T \bar{M}^{-1} (\hat{\bar{G}}(q) - \bar{G}(q)) - s^T \bar{M}^{-1} \bar{D}_f - s^T G_f f_s \\
&\quad + s^T \bar{M}^{-1} \bar{J}^T (\hat{N} - N)^T (-K_{dp}\dot{q} - K_{SL} \frac{\hat{\bar{M}}\hat{s}}{\| \hat{s} \| + \delta_{SL}}) - s^T \bar{M}^{-1} \Gamma_0 (\frac{s}{\| s \| + \delta})
\end{aligned}$$

This implies

$$\begin{aligned}
\dot{V}_s &\leq s^T \bar{M}^{-1} \left((\hat{\bar{M}} - \bar{M}) f^* + (\hat{\bar{V}}(q,\dot{q})\dot{r} - \bar{V}(q,\dot{q})\dot{r}) \right) \\
&\quad + s^T \bar{M}^{-1} (\hat{\bar{G}}(q) - \bar{G}(q)) - s^T \bar{M}^{-1} \bar{D}_f - s^T G_f f_s \\
&\quad + s^T \bar{M}^{-1} \bar{J}^T (\hat{N} - N)^T (-K_{dp}\dot{q} - K_{SL} \frac{\hat{\bar{M}}\hat{s}}{\| \hat{s} \| + \delta_{SL}}) - \Gamma_0 \frac{\lambda_{min}(\bar{M}^{-1}) \| s \|^2}{\| s \| + \delta} \\
&= s^T \bar{M}^{-1} \left((\hat{\bar{M}} - \bar{M}) f^* + (\hat{\bar{V}}(q,\dot{q})\dot{r} - \bar{V}(q,\dot{q})\dot{r}) \right) \\
&\quad + s^T \bar{M}^{-1} (\hat{\bar{G}}(q) - \bar{G}(q)) - s^T \bar{M}^{-1} \bar{D}_f - s^T G_f f_s \\
&\quad + s^T \bar{M}^{-1} \bar{J}^T (\hat{N} - N)^T (-K_{dp}\dot{q} - K_{SL} \frac{\hat{\bar{M}}\hat{s}}{\| \hat{s} \| + \delta_{SL}}) - \Gamma_0 \lambda_{min}(\bar{M}^{-1}) \| s \| \\
&\quad + \Gamma_0 \frac{\lambda_{min}(\bar{M}^{-1}) \| s \| \delta}{\| s \| + \delta}
\end{aligned}$$

and

$$\begin{aligned}
\dot{V}_s &\leq \left\| \bar{M}^{-1} \left((\hat{\bar{M}} - \bar{M}) f^* + (\hat{\bar{V}}(q,\dot{q})\dot{r} - \bar{V}(q,\dot{q})\dot{r}) \right) \right. \\
&\quad \left. + \bar{M}^{-1} (\hat{\bar{G}}(q) - \bar{G}(q)) - \bar{M}^{-1} \bar{D}_f - G_f f_s - \bar{M}^{-1} \bar{J}^T (\hat{N} - N)^T K_{dp} \dot{q} \right\| \| s \| \\
&\quad + \left\| \bar{M}^{-1} \bar{J} (\hat{N} - N)^T \right\| K_{SL} \| \hat{\bar{M}} \| \| s \| - \Gamma_0 \lambda_{min}(\bar{M}^{-1}) \| s \| + \Gamma_0 \lambda_{min}(\bar{M}^{-1}) \delta \\
&\leq \left(\left\| \bar{M}^{-1} \left((\hat{\bar{M}} - \bar{M}) f^* + (\hat{\bar{V}}(q,\dot{q})\dot{r} - \bar{V}(q,\dot{q})\dot{r}) \right) \right. \right. \\
&\quad \left. + \bar{M}^{-1} (\hat{\bar{G}}(q) - \bar{G}(q)) - \bar{M}^{-1} \bar{D}_f - G_f f_s - \bar{M}^{-1} \bar{J}^T (\hat{N} - N)^T K_{dp} \dot{q} \right\| \\
&\quad \left. + \left\| \bar{M}^{-1} \bar{J} (\hat{N} - N)^T \right\| K_{SL} \| \hat{\bar{M}} \| \right) \sqrt{2} \sqrt{V_s} \\
&\quad - \Gamma_0 \lambda_{min}(\bar{M}^{-1}) \sqrt{2} \sqrt{V_s} + \Gamma_0 \lambda_{min}(\bar{M}^{-1}) \delta.
\end{aligned}$$

Assuming

$$\Gamma_0 \lambda_{min}(\bar{M}^{-1}) \;>\; \Big\|\bar{M}^{-1}\Big((\bar{M}-\hat{\bar{M}})f^*+(\bar{V}(q,\dot{q})-\hat{\bar{V}}(q,\dot{q}))\dot{r}+\bar{G}(q)-\hat{\bar{G}}(q)+\bar{D}_f\Big)-G_f f_s \\ -\bar{M}^{-1}\bar{J}^T(\hat{N}-N)^T K_{dp}\dot{q}\Big\| + \Big\|\bar{M}^{-1}\bar{J}(\hat{N}-N)^T\Big\| K_{SL}\|\hat{\bar{M}}\| \tag{26}$$

and the assumption of $s(t=0)=0$, it is evident that the sliding variable s remains within a compact set for which the radius is proportional to δ. For $\delta = 0$, it follows that $s(t) = 0$ for all time $t > 0$. ■

The requirement of (26) provides excellent evidence why the integral sliding mode technique is almost model free; for instance, it is easily possible to assume for instance that the estimate for the Coriolis/centrifugal effects has been insufficiently modeled, i.e. $\hat{\bar{V}}(\cdot,\cdot) = 0$. This would create a higher demand on Γ_0 in (26).

It is to note, once $s(t) = 0$ is achieved, the task controller follows the ideal reference model of (9), representing an arbitrarily tunable mass-spring damper system subject to an external force f_s. Thus, Section 4 provides a practical discussion of this reference model, which is in particular suited to evaluate how well the reference model is practically followed in the actual implementation.

A.2. **Posture Motion.**

It has been emphasized that task motion takes priority over posture motion. Despite that, the posture controller is robust to model uncertainty, i.e. $\hat{s} = 0$ is achieved in case, $\delta_{SL} \to 0+$, which is summarized below using[40]:

Lemma 2. *If the matrix $M^{-1}\hat{M} + \hat{M}M^{-1}$ is strictly positive definite at all times, the variable, $\hat{s}$, is ultimately bounded, i.e. it will remain in a compact set, also containing $\hat{s} = 0$, after finite time. For $\delta_{SL} = 0$, $\hat{s} = 0$ is achieved within finite time.* •

The constraint for positive definiteness of $M^{-1}\hat{M} + \hat{M}M^{-1}$ is in principle an assumption that the mass estimate, $\hat{M}$, is fairly good, which can be assumed to be correct, considering the simplicity of the robot finger dynamics. In the ideal case, $M^{-1}\hat{M} + \hat{M}M^{-1} = 2I$. The proof of the lemma is based on[40]:

Proof: Consider $V_{\hat{s}} = \frac{1}{2}\hat{s}^T\hat{s}$, which implies from (1)

$$\begin{aligned}
\dot{V}_{\hat{s}} &= \hat{s}^T\dot{\hat{s}} \\
&= \hat{s}^T B(\ddot{q} + K_v(\frac{\partial^2 U}{\partial q^2}\ddot{q})^T) + \hat{s}^T\dot{B}(\dot{q} + K_v(\frac{\partial U}{\partial q})^T) \\
&= \hat{s}^T B(-M^{-1}V(q,\dot{q})\dot{q} - M^{-1}G(q) - M^{-1}D_f + M^{-1}\tau + K_v(\frac{\partial^2 U}{\partial q^2}\ddot{q})^T) \\
&\quad + \hat{s}^T\dot{B}(\dot{q} + K_v(\frac{\partial U}{\partial q})^T)
\end{aligned}$$

From $BB = B$ and (12) follows, $B\hat{s} = \hat{s}$. Moreover, defining $R = -M^{-1}V(q,\dot{q})\dot{q} - M^{-1}G(q) - M^{-1}D_f + K_v(\frac{\partial^2 U}{\partial q^2}\ddot{q})^T + \dot{B}(\dot{q} + K_v(\frac{\partial U}{\partial q})^T)$, it easily seen that

$$\dot{V}_{\hat{s}} = \hat{s}^T B(M^{-1}\tau + R) \tag{27}$$

Now, it is possible to exploit the relationships $N^T\hat{M}B = \hat{M}B$, $B\hat{s} = \hat{s}$ and $N^T B = N^T$, so that

$$\begin{aligned}
\dot{V}_{\hat{s}} &= -K_{dp}\hat{s}^T B M^{-1}\hat{N}^T B\hat{s} - K_{SL}\hat{s}^T B M^{-1}\hat{M}B\frac{\hat{s}}{\|\hat{s}\| + \delta_{SL}} \\
&\quad + \hat{s}^T(-K_{dp}K_v M^{-1}\hat{N}^T(\frac{\partial U}{\partial q})^T + BJ^T F + BR) \qquad (28)
\end{aligned}$$

Note that BJ^T and using the (positive) smallest eigenvalue $\lambda_{min}(\cdot)$ of $(M^{-1}\hat{M} + M^{-1}\hat{M})$:

$$\begin{aligned}
\dot{V}_{\hat{s}} &= -\hat{s}^T B M^{-1}N^T B\hat{s} - K_{SL}\frac{1}{2}\hat{s}^T B(M^{-1}\hat{M} + M^{-1}\hat{M})B\frac{\hat{s}}{\|\hat{s}\| + \delta_{SL}} \\
&\quad + \hat{s}^T(M^{-1}(N^T - \hat{N}^T)\hat{s} - K_{dp}K_v M^{-1}\hat{N}^T(\frac{\partial U}{\partial q})^T + BR) \\
&\leq -K_{SL}\lambda_{min}(M^{-1}\hat{M} + M^{-1}\hat{M})\frac{1}{2}\hat{s}^T\frac{\hat{s}}{\|\hat{s}\| + \delta_{SL}} \\
&\quad + \|\hat{s}\|\left\|(M^{-1}(N^T - \hat{N}^T)\hat{s} - K_{dp}K_v M^{-1}\hat{N}^T(\frac{\partial U}{\partial q})^T + BR)\right\| \\
&\leq -K_{SL}\lambda_{min}(M^{-1}\hat{M} + M^{-1}\hat{M})\frac{1}{\sqrt{2}}\sqrt{V_{\hat{s}}} \\
&\quad + \sqrt{2}\sqrt{V_{\hat{s}}}\|M^{-1}(N^T - \hat{N}^T)\hat{s} - K_{dp}K_v M^{-1}\hat{N}^T(\frac{\partial U}{\partial q})^T + BR\| \\
&\quad + K_{SL}\delta_{SL}\frac{1}{2}\lambda_{min}(M^{-1}\hat{M} + M^{-1}\hat{M}),
\end{aligned}$$

where the matrix $BM^{-1}N^TB$ is symmetric and positive semi-definite. Hence, for

(29)

$$K_{SL}\lambda_{min}(M^{-1}\hat{M}+M^{-1}\hat{M})\frac{1}{2} > \|M^{-1}(N^T-\hat{N}^T)\hat{s}-K_{dp}K_vM^{-1}\hat{N}^T(\frac{\partial U}{\partial q})^T+BR\|,$$

it is seen that $\hat{s}$ is entering a set of ultimate boundedness, where the radius is proportional to δ_{SL}. Hence, for $\delta_{SL}=0$, it is possible to achieve $\hat{s}=0$ within finite time. ■

REFERENCES

[1] S. Jacobsen, J. Wood, D. Knutti, and K. Biggers, "The utah/m.i.t. dextrous hand: Work in progress," *The International Journal of Robotics Research*, vol. 3, no. 4, pp. 21–50, 1984.

[2] ShadowRobot, "Design of a dextrous hand for advanced clawar applications," in *In Proceedings of CLAWAR*, 2003, pp. 691–698.

[3] M. Grebenstein, A. Albu-Schaffer, T. Bahls, M. Chalon, O. Eiberger, W. Friedl, R. Gruber, S. Haddadin, U. Hagn, R. Haslinger, H. Hoppner, S. Jorg, M. Nickl, A. Nothhelfer, F. Petit, J. Reill, N. Seitz, T. Wimbock, S. Wolf, T. Wusthoff, and G. Hirzinger, "The DLR hand arm system," in *Robotics and Automation (ICRA), 2011 IEEE International Conference on*, may 2011, pp. 3175 –3182.

[4] C. Borst, M. Fischer, S. Haidacher, H. Liu, and G. Hirzinger, "DLR hand ii: experiments and experience with an anthropomorphic hand," in *ICRA '03, Proceedings of the IEEE International Conference on Robotics and Automation*, vol. 1, Sept. 2003, pp. 702–707.

[5] W. B. Griffin, R. P. Findley, M. L. Turner, and M. R. Cutkosky, "Calibration and mapping of a human hand for dexterous telemanipulation," in *ASME IMECE 2000 Symposium on Haptic Interfaces for Virtual Environments and Teleoperator Systems*, 2000, pp. 1–8.

[6] D. Akin, C. Carignan, and A. Foster, "Development of a four-fingered dexterous robot end effector for space operations," in *IEEE International Conference on Robotics and Automation*, vol. 3, 2002, pp. 2302 –2308.

[7] T. Geng, M. Lee, and M. Hlse, "Transferring human grasping synergies to a robot," *Mechatronics*, vol. 21, no. 1, pp. 272 – 284, 2011.

[8] H. Wang, K. H. Low, M. Y. Wang, and F. Gong, "A mapping method for telemanipulation of the non-anthropomorphic robotic hands with initial experimental validation," in *Proceedings of the 2005 IEEE International Conference on Robotics and Automation, 2005. ICRA 2005.* IEEE, 2005, pp. 4218–4223.

[9] G. Gioioso, G. Salvietti, M. Malvezzi, and D. Prattichizzo, "Mapping synergies from human to robotic hands with dissimilar kinematics: An approach in the object domain," *IEEE Transactions on Robotics*, vol. 29, no. 4, pp. 825–837, 2013.

[10] S. C. Bae, "Investigation of hand posture during reach and grasp for ergonomic applications," Doctor of Philosophy, University of Michigan, 2011.

[11] J. Jalani, N. Mahyuddin, G. Herrmann, and C. Melhuish, "Active robot hand compliance using operational space and integral sliding mode control," in *IEEE/ASME International Conference on Advanced Intelligent Mechatronics (AIM), 2013*, 2013, pp. 1749–1754.

[12] J. Jalani, G. Herrmann, and C. Melhuish, “Robust active compliance control for practical grasping of a cylindrical object via a multifingered robot hand,” in *2011 IEEE Conference on Robotics, Automation and Mechatronics (RAM)*, 2011, pp. 316–321.

[13] V. DeSapio, J. Warren, O. Khatib, and S. Delp, “Simulating the task-level control of human motion: a methodology and framework for implementation.” *The Visual Computer*, pp. 289–302, 2005.

[14] B. Siciliano, L. Sciavicco, L. Villani, and G. Oriolo, *Robotics: Modelling, Planning and Control*. Springer, 2008.

[15] R. Ham, T. Sugar, B. Vanderborght, K. Hollander, and D. Lefeber, “Compliant actuator designs,” *Robotics Automation Magazine, IEEE*, vol. 16, no. 3, pp. 81 –94, september 2009.

[16] M. R. Cutkosky, *Robotic Grasping and Fine Manipulation*. Norwell, MA, USA: Kluwer Academic Publishers, 1985.

[17] K. L. Johnson, *Contact Mechanics*. Cambridge, UK: Cambridge University Press, Cambridge, 1985.

[18] K. Shimoga and A. Goldenberg, “Soft robotic fingertips,” *The International Journal of Robotics Research*, vol. 15, no. 4, pp. 320–334, 1996.

[19] L. Biagiotti, C. Melchiorri, P. Tiezzi, and G. Vassura, “Modelling and identification of soft pads for robotic hands,” in *IEEE/RSJ International Conference on Intelligent Robots and Systems (IROS)*, 2005.

[20] T. L. Lionel Birglen, Clment Gosselin, *Underactuated Robotics Hand*. Springer-Verlag, Berlin Heidelberg, 2008.

[21] H. BenAmor, A. Saxena, N. Hudson, and J. Peters, “Special issue on autonomous grasping and manipulation,” *Autonomous Robots*, vol. 36, no. 1-2, pp. 1–3, 2014.

[22] H. Liu and G. Hirzinger, “Cartesian impedance control for the DLR hand,” in *Intelligent Robots and Systems, 1999. IROS ’99.*, vol. 1, 1999, pp. 106 –112.

[23] C. Ott, A. Albu-Schaffer, A. Kugi, and G. Hirzinger, “On the passivity-based impedance control of flexible joint robots,” *IEEE Transactions on Robotics*, vol. 24, no. 2, pp. 416 –429, 2008.

[24] A. Albu-Schaffer, C. Ott, and G. Hirzinger, “A unified passivity-based control framework for position, torque and impedance control of flexible joint robots,” *The International Journal of Robotics Research*, vol. 26, no. 1, pp. 23–39, 2007.

[25] S. Khan, G. Herrmann, A. Pipe, and C. Melhuish, “Safe adaptive compliance control of a humanoid robotic arm with anti-windup compensation and posture control,” *International Journal of Social Robotics*, vol. 2, no. 3, pp. 305–319, 2010.

[26] Z. Chen, N. Lii, T. Wimboeck, S. Fan, M. Jin, C. Borst, and H. Liu, “Experimental study on impedance control for the five-finger dexterous robot hand DLR-HIT ii,” in *2010 IEEE/RSJ International Conference on Intelligent Robots and Systems (IROS)*, 2010, pp. 5867 –5874.

[27] K. Mouri, K. Terashima, P. Minyong, H. Kitagawa, and T. Miyoshi, “Identification and hybrid impedance control of human skin muscle by multi-fingered robot hand,” in *IROS 2007. IEEE/RSJ International Conference on Intelligent Robots and Systems, 2007.*, 2007, pp. 2895 –2900.

[28] Y. Xu and R. Paul, “On position compensation and force control stability of a robot with a compliant wrist,” in *Robotics and Automation, 1988. Proceedings., 1988 IEEE International Conference on*, vol. 2, April 1988, pp. 1173 –1178 vol.2.

[29] A. Jaura, M. Osman, and N. Krouglicof, “Hybrid compliance control for intelligent assembly in a robot work cell,” *International Journal of Production Research*, vol. 36, no. 9, pp. 2573–2583, 1998.

[30] B.-H. Kim, S.-R. Oh, I. Suh, and g.-J. Yi, “A compliance control strategy for robot manipulators under unknown environment,” *KSME International Journal*, vol. 14, pp. 1081–1088, 2000.

[31] S. Khan, G. Herrmann, T. Pipe, and C. Melhuish, “Adaptive multi-dimensional compliance control of a humanoid robotic arm with anti-windup compensation,” in *2010 IEEE/RSJ International Conference on Intelligent Robots and Systems (IROS)*, 2010, pp. 2218–2223.

[32] S. Haddadin, F. Huber, K. Krieger, R. Weitschat, A. Albu-Schaffer, S. Wolf, W. Friedl, M. Grebenstein, F. Petit, J. Reinecke, and R. Lampariello, “Intrinsically elastic robots: The key to human like performance,” in *2012 IEEE/RSJ International Conference on Intelligent Robots and Systems (IROS)*, 2012, pp. 4270–4271.

[33] C. Ott, B. Henze, and D. Lee, “Kinesthetic teaching of humanoid motion based on whole-body compliance control with interaction-aware balancing,” in *2013 IEEE/RSJ International Conference on Intelligent Robots and Systems (IROS)*, 2013, pp. 4615–4621.

[34] H. Sadeghian, M. Keshmiri, L. Villani, and B. Siciliano, “Null-space impedance control with disturbance observer,” in *Intelligent Robots and Systems (IROS), 2012 IEEE/RSJ International Conference on*, 2012, pp. 2795–2800.

[35] T. Zhang, L. Jiang, S. Fan, X. Wu, and W. Feng, “Development and experimental evaluation of multi-fingered robot hand with adaptive impedance control for unknown environment grasping,” *Robotica*, vol. FirstView, pp. 1–18, 10 2014.

[36] T. Zhang, L. Jiang, X. Wu, W. Feng, D. Zhou, and H. Liu, “Fingertip three-axis tactile sensor for multifingered grasping,” *IEEE/ASME Transactions on Mechatronics*, vol. PP, no. 99, pp. 1–11, 2014.

[37] T. Zhang, H. Liu, L. Jiang, S. Fan, and J. Yang, “Development of a flexible 3-d tactile sensor system for anthropomorphic artificial hand,” *IEEE Sensors Journal*, vol. 13, no. 2, pp. 510–518, 2013.

[38] J. Shi, H. Liu, and N. Bajcinca, “Robust control of robotic manipulators based on integral sliding mode,” *International Journal of Control*, vol. 81, pp. 1537–1548, 2008.

[39] J. Jalani, G. Herrmann, and C. Melhuish, “Underactuated fingers controlled by robust and adaptive trajectory following methods,” *International Journal of Systems Science*, 2012.

[40] A. Spiers, G. Herrmann, and C. Melhuish, “An optimal sliding mode controller applied to human motion synthesis with robotic implementation,” in *American Control Conference (ACC)*, 30 2010-July 2 2010, pp. 991 –996.

[41] J. Jalani, G. Herrmann, and C. Melhuish, “Robust trajectory following for underactuated robot fingers,” in *UKACC International Conference on CONTROL 2010*, September 2010, pp. 495–500.

[42] O. Khatib, “A unified approach for motion and force control of robot manipulators: The operational space formulation,” *IEEE Journal of Robotics and Automation*, vol. 3, no. 1, pp. 43 –53, 1987.

[43] ——, “Inertial properties in robotic manipulation: An object-level framework,” *The International Journal of Robotics Research*, vol. 14, no. 1, pp. 19–36, 1995.

[44] M. Yokoyama, G.-N. Kim, and M. Tsuchiya, “Integral Sliding Mode Control with Anti-windup Compensation and Its Application to a Power Assist System,” *Journal of Vibration and Control*, vol. 16, no. 4, pp.

503–512, 2010.

[45] M. Defoort, T. Floquet, A. Kokosy, and W. Perruquetti, “Integral sliding mode control for trajectory tracking of a unicycle type mobile robot,” *Integr. Comput.-Aided Eng.*, vol. 13, no. 3, pp. 277–288, 2006.

[46] I. Eker and S. Akinal, “Sliding mode control with integral augmented sliding surface: design and experimental application to an electromechanical system,” *Electrical Engineering (Archiv fur Elektrotechnik)*, vol. 90, no. 3, pp. 189–197, 2008.

[47] Pressure Profile Systems, Inc. ConTacts C500 Single-Point Tactile Sensor. [Online]. Available: test